

Article

Austenite Formation in the Oxidized Layer of Ultra-High-Strength 13Ni15Co10Mo Maraging Steel

Daniela P. M. da Fonseca ^{1,*} , Leandro G. de Carvalho ², Nelson B. de Lima ³ and Angelo F. Padilha ¹

¹ Departamento de Engenharia Metalúrgica e de Materiais, Escola Politécnica da Universidade de São Paulo (EP-USP), São Paulo 05508-030, Brazil

² Departamento de Computação, Centro Universitário Adventista de São Paulo (UNASP), São Paulo 05858-001, Brazil

³ Instituto de Pesquisas Energéticas e Nucleares (IPEN-CNEN/SP), São Paulo 05508-000, Brazil

* Correspondence: danipassarelo@usp.br

Abstract: Maraging steels are precipitation hardening alloys that can achieve an ultra-high yield strength (~3 GPa), however associated with low toughness. During exposure to high temperatures, an oxidation process occurs on the surface of these steels, generally, the oxides formed are hematite and/or magnetite. The aim of this study was to investigate oxidation on a maraging 13Ni15Co10Mo at annealing temperature of 900 °C. The bulk microstructure was investigated by several complementary techniques and the oxidized surface was characterized by Scanning Electron Microscopy (SEM), Energy Dispersive X-ray Spectroscopy (EDS) and X-ray Diffraction (XRD). The results showed that the bulk microstructure, at annealed condition, consists of a lath martensite with a hardness of round 400 HV. The most external and oxidized surface contains the oxides hematite, magnetite and kaminokite. Finally, the presence of austenite was detected in the first 2 µm below the surface. Chemical microanalysis indicated that the austenite is stable at room temperature in this region due a composition gradient that makes this region rich in nickel and cobalt. The composition gradient is due atom diffusion during oxides formation. Austenite near to the surface is very convenient as it could avoid crack initiation and propagation, improving toughness.

Keywords: austenite; maraging steel; maraging 13Ni15Co10Mo; oxidation; oxides



Citation: Fonseca, D.P.M.d.; Carvalho, L.G.d.; Lima, N.B.d.; Padilha, A.F. Austenite Formation in the Oxidized Layer of Ultra-High-Strength 13Ni15Co10Mo Maraging Steel. *Metals* **2022**, *12*, 2115. <https://doi.org/10.3390/met12122115>

Academic Editors: Joan-Josep Suñol and Andrey Belyakov

Received: 4 November 2022

Accepted: 7 December 2022

Published: 9 December 2022

Publisher's Note: MDPI stays neutral with regard to jurisdictional claims in published maps and institutional affiliations.



Copyright: © 2022 by the authors. Licensee MDPI, Basel, Switzerland. This article is an open access article distributed under the terms and conditions of the Creative Commons Attribution (CC BY) license (<https://creativecommons.org/licenses/by/4.0/>).

1. Introduction

Maraging steels are an unconventional class of precipitation hardened ultra-high mechanical strength steels. Indispensable elements in traditional steels like carbon, silicon and manganese are residual elements in maraging steels. They are based on the Fe-Ni-Co-Mo system and show an unparalleled combination of excellent manufacturability, high strength and fracture toughness [1].

Commercial maraging steels are named according to their level of yield strength (200 to 400 ksi) they can present in the aged condition. The most common maraging steels (maraging 200, 250, 300 and 350) have Fe-18.5Ni (wt.%) as base composition, with increasing molybdenum levels from 3.3–5.0 wt.%, cobalt levels from 8.5–12.5 wt.% and titanium levels of 0.2–1.6 wt.% [2]. To be able to achieve higher levels of mechanical strength, such as yield strength of around 3 GPa, the base composition had to be changed to Fe-13Ni-15Co-10Mo-1Ti (wt.%) [3–6].

The high levels of mechanical strength are due to precipitation of intermetallic compounds such as Ni₃(Ti, Mo) and Fe₂Mo in a low carbon and soft BCC martensitic matrix obtained by air cooling after solution annealing (austenitization) [7]. The increase in mechanical strength that occurs during aging is associated with the sharp drop in toughness. For example, for a maraging 350, while the yield strength changes from 935 MPa after solution annealing to 2195 MPa at hardness peak after aging, the energy absorbed in the Charpy impact test drops from 190 to 12 J [7]. The K_{IC} (MPa m^{1/2}) value of a maraging 250

is more than twice that of a maraging 350 [2]. In the case of maraging 400, the toughness drop is even more critical [3,4,8]. One of the ways to increase toughness is the overaging, when coarsening of precipitate particles and partial reversion of martensite into austenite occurs [2]. However, the drop in yield strength is a negative consequence of the overaging heat treatments.

Systematic studies of protective films on austenitic stainless steels [9–12] and mild steels [13], however similar studies on maraging steels are scarce.

The corrosion resistance of maraging steels is nothing special, or more precisely, it is slightly better than the corrosion resistance of high-strength low-alloy (HSLA) steels. On the other hand, their oxidation resistance is substantially better than that of low-alloy steels [2]. Oxidation of maraging 250 and 300 has been studied in water steam, nitrogen/water vapor, carbon dioxide and oxygen between 300 and 600 °C [14–22]. For instance, after 90 min at 540 °C a commercial grade maraging 300 presents an oxidized layer with three regions comprising CoO- α -Fe₂O₃, α -Fe₂O₃ and mixed spinel oxide phases, respectively. The oxide film grows by means of the outward diffusion of metal cations. Oxidation significantly changes the chemical composition of steel in the region just below the oxide layer, making austenite formation possible in this region. Oxidation studies in maraging 400 are very rare but necessary as they have a significantly different chemical composition than traditional maraging steels 200, 250, 300 and 350. Vicente and co-authors [23] studied the oxidation of maraging 400 steels during the homogenization heat treatment around 1250 °C. This high temperature is relevant from the steel processing point of view, but not directly related to its use. As maraging steel components are used in the hardened condition, solution annealing temperatures (800–900 °C) and aging (around 500 °C) are also important. Thus, the aim of this work was to study the oxidation of a maraging steel 13Ni15Co10Mo after solubilization at 900 °C.

2. Materials and Methods

A non-commercial maraging 400 steel was fabricated by vacuum induction melting (VIM) and electroslag remelting (ESR) with chemical composition presented at Table 1. The ingot was homogenized at 1250 °C for 5 h, forged and hot rolled. Then, the final samples were solution annealed at 900 °C for 1 h and cooled in air.

Table 1. Chemical Composition of the maraging steels (wt.%).

Fe	Ni	Co	Mo	Ti	Al	Si	Mn	C
Bal.	12.85	15.64	10.49	0.721	0.052	0.040	0.040	0.016

It was studied oxidized sheets with 30 × 30 mm and thickness of 1.25 mm. It was characterized three regions through normal direction (z), with different depth: (a) external layer—as received, without any preparation; (b) intermediate layer—superficial sanded, until get off external layer and (c) bulk—polished, complete metallography preparation.

Micrographs of bulk region were obtained by Optical Microscopy (OM), Scanning Electron Microscopy (SEM) (FEG FEI Inspect 50—USP, São Paulo-SP, Brazil) and Scanning Transmission Electron Microscopy (STEM) (JEOL 2100 F, 200 kV—LBNL, Berkeley-CA, US). Samples were cut, embedded in an epoxy resin, grinded, polished (3 μ m and 1 μ m diamond) and etched with Vilella's reagent (1 g picric acid, 5 mL HCl and 100 mL ethanol). The STEM specimens were prepared by FIB (FEI DualBeam Helios NanoLab 650—INMETRO, Xerém-RJ, Brazil). The dilatometry was carried out in a DIL 805 A/D dilatometer (USP, São Paulo-SP, Brazil) using cylindrical samples with 4 mm in diameter and 10 mm in length. The samples were heated to 1200 °C at a heating rate of 1 °C/s held at that temperature for 10 min, and then cooled to room temperature. The cooling rates were 1 °C/s up to 400 °C and 10 °C/s thereafter to room temperature. Vickers hardness measurements were made under a load of 1 kg for 15 s.

The semiquantitative analysis of the chemical composition was conducted by Energy Dispersive X-ray Spectroscopy (EDS) (EDAX). For each region (a, b and c), it was collected EDS data in three areas of $185 \times 185 \mu\text{m}$ and then it was calculated the mean and standard deviation. X-ray Diffraction (XRD) measurements were performed using a Rigaku Multiflex diffractometer equipped (IPEN, São Paulo-SP, Brazil). Data collection was conducted using copper $K\text{-}\alpha_1$ radiation in a 2θ range of $20\text{--}90^\circ$ using a step interval of 0.08° . For intermediate thin layer, it was applied complementary analyses by Grazing Incidence X-ray Diffraction (GIXRD) for angles of 3° , 5° , 7° , 10° and 12° . The Rietveld method was used to calculate the weight fractions of oxides, the refinement was carried out using GSAS software.

3. Results and Discussion

When exposed to high temperatures as during homogenizing (1250°C) and annealing (900°C), the maraging steel 13Ni15Co10Mo undergoes oxidation on its surface. To make the presentation of the results didactic and clear, as well as to better understand the microstructure resulting from the oxidation and the phases formed on the surface, it was characterized three regions through normal direction (z), with different depth. To help the results presentation, each region was named as: (a) External layer; (b) Intermediate layer and (c) Bulk. Figure 1 shows a schematic illustration of the studied regions. Figure 1a shows sheet illustration of the sample used and indicates the directions orientation. Figure 1b shows a cross section SEM(BSE) image at the y direction, containing the three layers, even if they are not quite individually distinguished, as will be explained later. It also shows some evidence of internal oxidation. Because backscattering electrons (BSE) was used to generate the images, it is possible to see dark and light grey regions in the first $1.7 \mu\text{m}$ of depth, this is the estimated depth of the oxidized surface. Figure 1c shows SEM(BSE) image at the z direction (external layer as received) where it can be seen a light gray region rich in molybdenum and a dark gray region rich in iron. Figure 1d shows SEM(SE) image of the bulk microstructure (z direction), showing a characteristic martensite morphology.

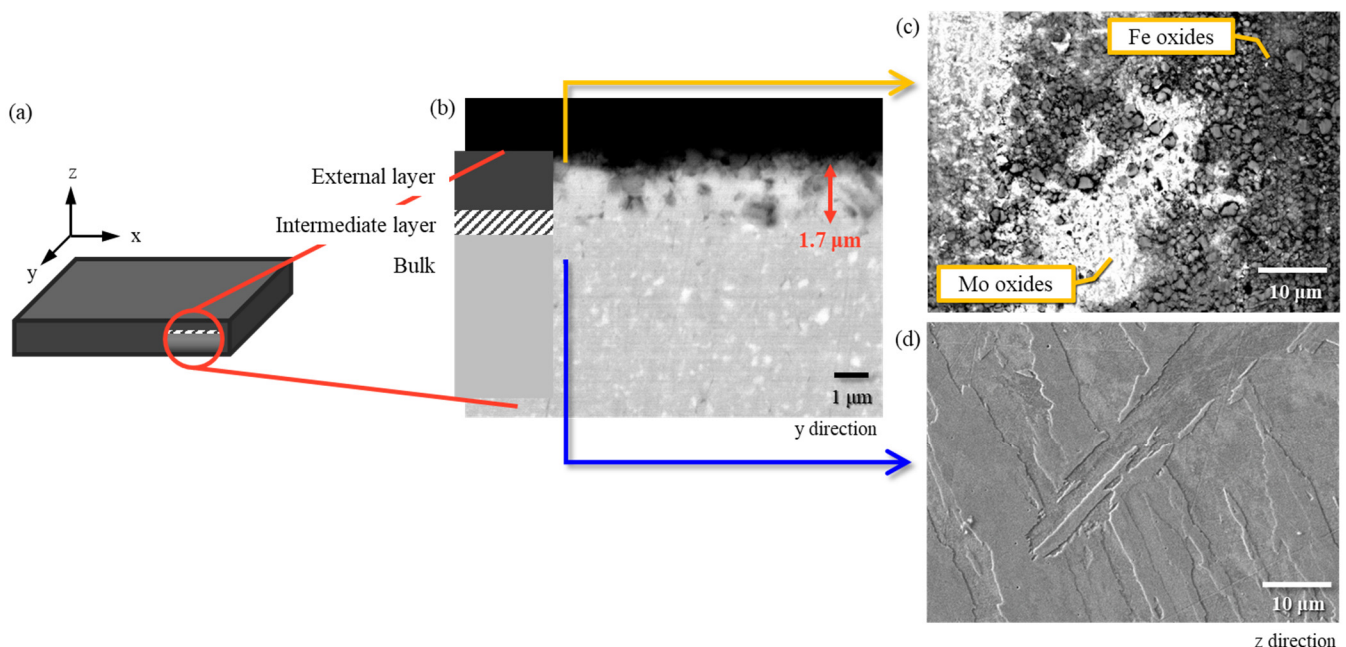


Figure 1. Schematic illustration of the studied regions: External layer, Intermediate layer and Bulk. (a) Sheet illustration and directions orientation; (b) SEM(BSE) image of the cross section (y direction), annealed sample as polished; (c) SEM(BSE) image of the external layer (z direction), light gray region is rich in molybdenum and dark gray region is rich in iron, annealed sample without any preparation (d) SEM(SE) image of the bulk (z direction) showing the martensite microstructure, annealed sample polished and etched.

A detailed microstructural characterization was performed in the bulk region, as this region represents the largest area of the material and, consequently, has the greatest influence on its behavior and properties. Then, each region (external layer, intermediate layer and bulk) was characterized individually and simultaneously.

3.1. Bulk Microstructure

The most used heat treatments for maraging steels are: homogenizing, annealing/austenitization (followed by cooling in air) and aging. The main objective of the homogenization heat treatment is the reduction of micro-segregation from the solidification step.

The heat treatments, beside generating surface oxidation, are also crucial on the properties control and performance of maraging steels. The metastable Fe-Ni phase diagram proposed for maraging steels containing Ti, Mo and Co [24] presents several temperature ranges with the respective phase transformations: (a) FCC austenite solid solution region at higher temperatures; (b) BCC martensite after quenching; (c) precipitation hardening of the martensite by small intermetallic precipitates during aging; and (d) overaging and reversed austenite. During the solution annealing, the material needs temperatures enough to achieve the austenite field and held for a certain time so that the solute atoms can diffuse throughout the material and form a single-phase solid solution. For maraging Fe-18Ni the ideal temperature is 820 °C, however, for maraging Fe-13Ni is necessary temperatures in the range of 900–1200 °C, this was noted by previous experimental studies of this authors, and it was suggested prior by some works at the literature [2–4]. After cooling in air until the room temperature, the material had a supersaturated and metastable solid solution (100% martensite) with BCC structure. During the aging occurs the precipitation hardening by the formation of nanometric intermetallic precipitates. The mechanical properties are controlled by the aging time and temperature, the peak hardness can be achieved for 3–6 h at 480 °C [5]. For longer times or higher temperatures, the overaging starts to occur leading to dispersion hardening and reversion of austenite [24].

Figure 2 shows images of OM, SEM and STEM for samples of maraging 13Ni15Co10Mo after annealing at 900 °C for 1 h and cooling in air. The images show the typical martensite microstructure (illustrated at Figure 2a) defined by packet, blocks, laths and a high density of dislocation tangles. The results indicated a very well dissolution of the micrometric precipitates (Fe_3Mo) remained after homogenizing.

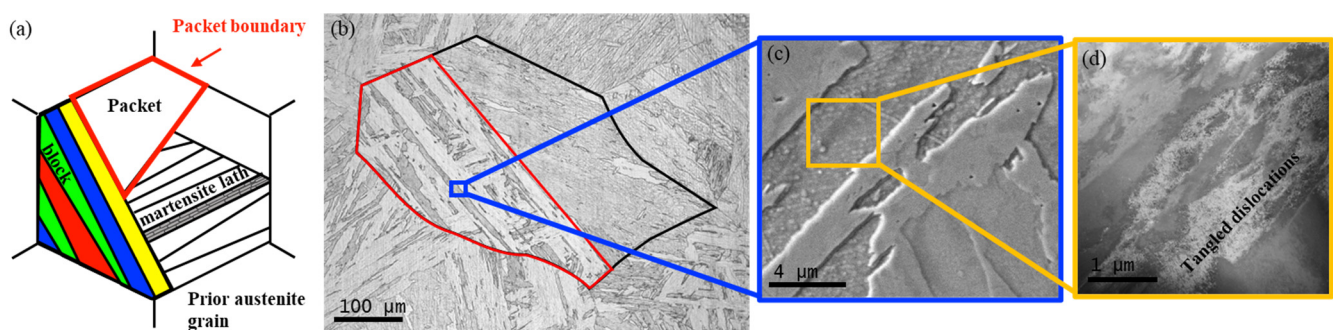


Figure 2. (a) Schematic illustration, (b) MO image, (c) SEM(SE) image and (d) STEM image of martensite microstructure of maraging 13Ni15Co10Mo annealed at 900 °C for 1 h and cooled in air. OM and SEM samples were etched with Vilella’s reagent.

Figure 3 shows the dilatometric heating and cooling curve obtained from an annealed sample. The percentage of change in length of the sample was plotted against temperature. Different characteristic temperatures obtained during the experiment are marked in red on the curve. During heating, uniform expansion continues until 579 °C when a very subtle contraction starts to occur, indicating the start of precipitation (P_s) at this temperature [25]. This is followed by a small period of linear expansion with increasing temperature at 632 °C, indicating the precipitation finish (P_f). The austenite reversion starts (A_s) soon after,

at 696 °C, and finishes (A_f) at 867 °C. Thereafter, the curve moves up as the temperature of the specimen is raised up to 1200 °C. The cooling curve of the specimen is shown below the heating curve without any relevant changes in the contraction rates up to 183 °C which is the martensite transformation start temperature (M_s). At around 50 °C the martensite transformation finishes (M_f). This result shows that the annealing temperature for maraging 13Ni15Co10Mo is above than for maraging steels 18Ni. The annealing temperature of 900 °C, used for the samples of this study, was adequate and above the necessary temperature for the complete austenite reversion.

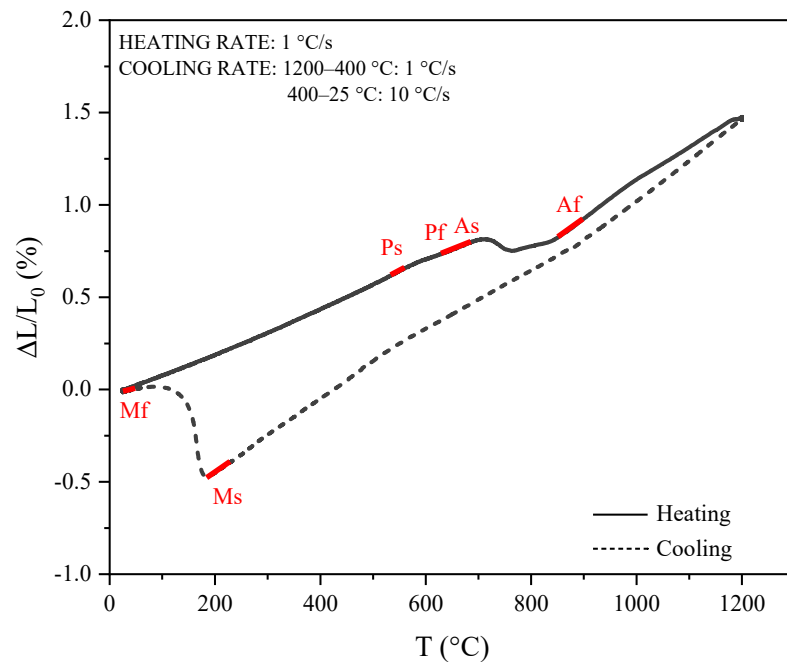


Figure 3. Dilatometry heating and cooling curves for the maraging 13Ni15Co10Mo showing transformation temperatures.

The samples at the condition homogenized, annealed and aged (at 480 °C for 3 h) showed hardness of 486 ± 12 HV1, 401 ± 6 HV1 and 774 ± 10 HV1, respectively. The hardness decreasing after annealing is due the dissolution of the micrometric precipitates Fe_3Mo . Although they are not the coherent and/or semi-coherent precipitates responsible for the ultra-high-strength of maraging (precipitation hardening), they lightly improve the hardness by dispersion hardening. The annealing is very important to dissolve these precipitates and the inclusions, ensuring that there is maximum solute in solid solution as the driving force for precipitation. After aging, the hardness increases 193%. This mean that the oxidation process, because it occurs just a few micrometers from the surface, does not affect the bulk composition and, consequently, does not have influence in the improvement of mechanical strength.

3.2. External, Intermediate and Bulk Microstructure

Figure 4 shows the XRD profiles at z direction from three different depths of the material: external layer (Figure 4a), intermediate layer (Figure 4b) and Bulk (Figure 4c). All diffractograms show expected peaks of the martensite BCC matrix. The more pronounced width of the martensite peaks should be associated with the high concentration of crystalline defects, mainly dislocations, in this phase [26–28]. The external layer (Figure 4a) exhibits the presence of the oxides hematite (Fe_2O_3), magnetite (Fe_3O_4) and kamiokite ($Fe_2Mo_3O_8$). From the external and intermediate layer, intensive peaks of FCC austenite we also identified, indicating the presence of this phase near to the surface. Austenite could not have been induced by mechanical deformation during metallography preparation of the intermediate layer samples (which was grinded to remove the external layer), as it

was detected also in the external layer (without preparation). It was made the Rietveld refinement of the XRD data from the external layer. Although the analysis was performed on the external layer, due to the depth of X-ray penetration, the diffractogram information comes from the three layers (a, b and c). The volumetric phase quantification calculated for hematite, magnetite, kamiokite, martensite and austenite showed 5.4%, 15%, 9.2%, 19% and 51.4%, respectively. That is, considering external and intermediate layer together, there is on the surface 51.4 vol.% of austenite, in a region of around 1.7 μm thick.

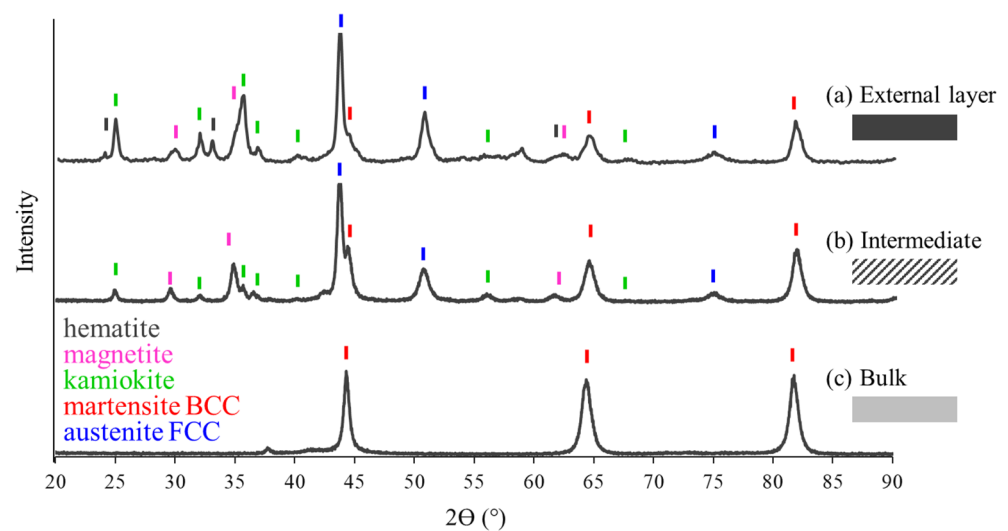


Figure 4. XRD profiles of each region at z direction. (a) external layer, (b) intermediate layer and (c) Bulk.

Figure 5 shows the XRD profile from analysis using grazing incidence X-ray at z direction of intermediate layer, from near to surface (3°) to bulk direction (until 12°). With the most grazing angle (3°), in red, there are only austenite peak and some oxides peaks. The martensite peak ($2\theta \sim 44.5^\circ$) just starts to show for 5° grazing angle (in green). It indicates that the austenite is present in a thin layer, between the oxide layer and the matrix.

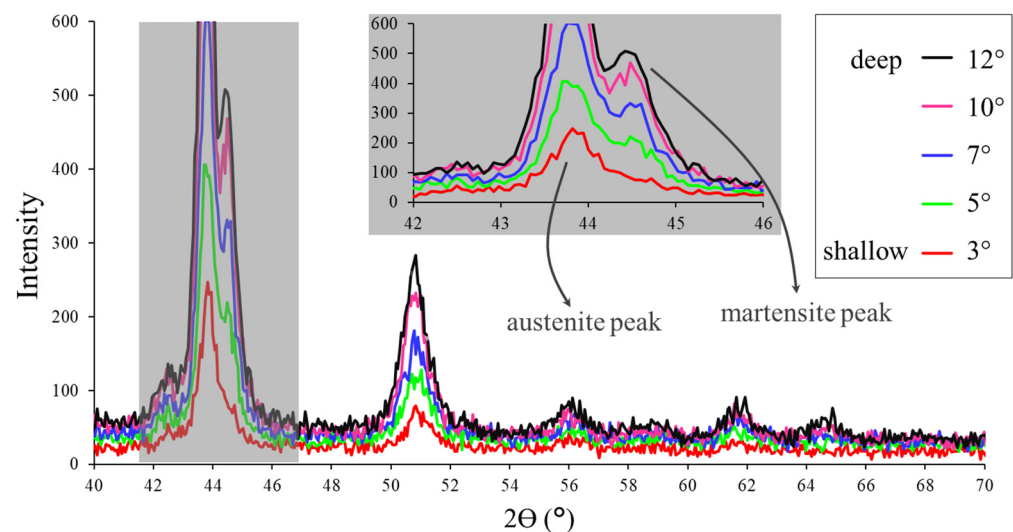


Figure 5. GIXRD profiles of intermediate layer at z direction varying incidence angles from 3° (shallow) to 12° (deeper). There is austenite peak for the shallowest angle (3° curve) and peaks of austenite and martensite for greater angles (deeper penetration in the sample).

Figure 6 presents a qualitative graph of composition of the main alloy elements (Fe, Ni, Co, Mo, Ti) through the material, obtained by EDS analysis on z direction of each region:

(a) external layer, (b) intermediate layer and (c) Bulk. The external layer is formed by three oxides (that were identified by XRD analysis, Figure 4), but on SEM analysis it was possible to distinguish just two regions: one dark grey, referent to the oxides rich in iron (hematite and magnetite), and other light gray, referent to oxide rich in molybdenum (kamiokite). That is why there are these error bars for Fe and Mo, even collecting data from areas of $185 \times 185 \mu\text{m}$ multiple times. Even though the EDS are a semi-quantitative analysis, the percentage of the elements from bulk are very close to the composition of the alloy, except for Mo. In the EDS quantification of these maraging steels, the molybdenum element presents a slightly lower content than the real one. This happens because, for molybdenum, only the X-rays characteristic of the L shell (less energetic than the K-layer) are used, while for the other elements, characteristic X-rays of the K and L shell are detected. After stoichiometric calculations it was estimated that the percentages of molybdenum obtained by the quantification of EDS is about 23% lower than the real one. The continuous red line indicates the values measured by EDS, the dotted red line represents an estimate of the real fraction of molybdenum.

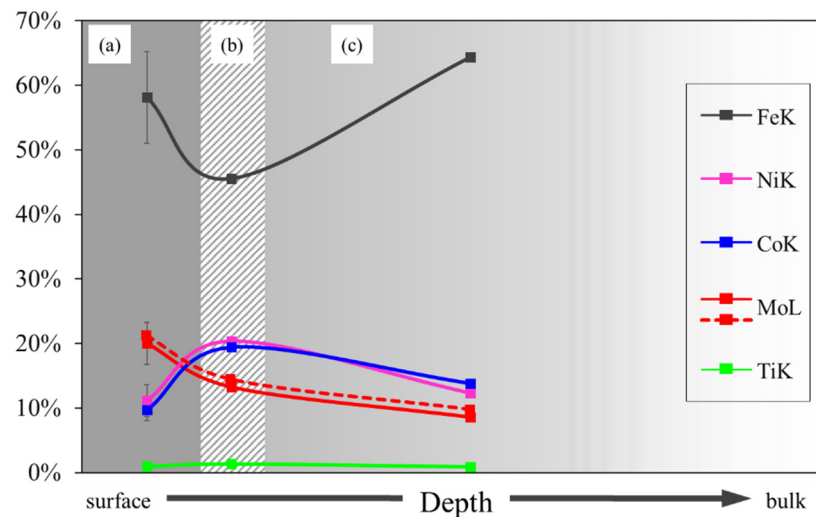


Figure 6. Qualitative composition of the elements by EDS microanalysis along the depth of the sample: (a) external layer, (b) intermediate layer and (c) Bulk. Several EDSs were obtained independently in each layer from z direction and then the results were compiled in this figure. The intermediate layer is rich in nickel and cobalt, austenite stabilizers.

During exposure to high temperatures, most of the molybdenum atoms that are close to the surface react with iron and the atmosphere, forming the $\text{Fe}_2\text{Mo}_3\text{O}_8$ oxide (kamiokite). According to Klein and co-authors [14], the formation of nickel (NiFe_2O_4) and cobalt (CoFe_2O_4) oxides is unlikely, so it can be assumed that, during the formation of iron and molybdenum oxides, in the border region between the external and intermediate layers, there is a thin region rich in nickel and cobalt, which diffused towards the bulk. In the intermediate layer (Figure 6b) the actual molybdenum content is more than 13% (about 17%), the nickel content is 20%, the cobalt content is 19% and the iron content is 45%. Previous work carried out by Khan and co-authors also confirms the presence of a multilayer iron and molybdenum oxides during the oxidation of a maraging 350 steel in air at temperature range 900–1350 °C. EDS analysis confirms that the intermediate oxide layer had a content 9% of molybdenum, 28% of nickel, 16% of cobalt, and 44% iron [29].

Bourgeot and co-authors [30] presented a metastable experimental diagram showing the phase fields of Fe-Ni-Mo alloys after quenching from 1100, 1200 and 1250 °C. For our bulk composition of 10.49 wt.%Mo and 12.85 wt.%Ni, according to their diagram, there is the presence of only martensite phase after quenching from 1100 °C. However, for the composition of our intermediate layer (13–17 wt.%Mo and 20 wt.%Ni), there is the presence of only the austenite phase. The diagram was drawn without considering

the presence of cobalt, but since Co is an austenite stabilizer element, for our alloy (containing 15.64 wt.%Co) the high-temperature austenite field is possibly even larger than that obtained by Bourgeot and co-authors and the full martensitic microstructure after quenching predictable.

Austenite is not a stable phase at room temperatures in maraging steels. The calculated values of Ms and Mf corroborate this, where the martensite transformation finishes around 50 °C [25]. The oxidation process causes changes in the local and superficial composition that allow austenite stabilization at room temperature. This oxidation occurred due air exposure at high temperatures during the heat treatment of annealing (900 °C). This process also happens during high temperatures exposure of others maraging steel grades (18Ni). The literature has been recurrently reporting the formation of hematite and magnetite in these materials [14–17]. However, it was not found in the literature any indication of kamiokite formation. Most studies did not even identify oxides containing molybdenum, Pfistermeister and co-authors [22] claimed to detect iron (ii) molybdate (FeMoO_4) and Florez and co-authors identified molybdenum oxide MoO_3 [31]. Apparently, the formation of kamiokite is a particular case of maraging 13Ni15Co10Mo, due its higher molybdenum content.

The distribution of the oxides, austenite and martensite phases along the thickness (from external surface towards the bulk) is not easy to distinguish. They can be distributed as overlapped layers (oxides, austenite then martensite) or as single layer with a mixture distribution of these multiple phases. The literature reports that even the oxides can be distributed in overlapped layers [17]. However, the results obtained in this work suggest that very close to the surface there is a thin layer consisting of oxides and austenite. Followed by a transition layer consisting of oxides, austenite and martensite. The oxide region seems to end abruptly, while the austenite region seems to be gradually transforming into martensite. The thickness of the region containing oxides is around 1.7 μm .

From the perspective of a wide industrial application, the low toughness has been a limitation for maraging 13Ni15Co10Mo in the aged condition. A superficial layer made by the combination of ductile austenite and oxides, in overlapped layers or single layer of multiple phases, can hinder the crack initiation and also be a barrier against extreme environments.

Since maraging steels are precipitation hardened alloy, it is important to point that the commercial standard condition for such material is annealed and aged. The results obtained indicated that oxidation processes during annealing do not influence the bulk hardness improvement during aging. However, the results also showed that there is a composition gradient a few micrometers from the surface. It is worth producing future studies about the precipitation behavior in this region.

4. Conclusions

There is very little information in the literature about the oxidation behavior of this class of maraging steel at a very important temperature, in which the material is solution annealed before aging, therefore, making many of the results of this paper a novelty. The following conclusions could be drawn from the present work on the microstructural characterization of the bulk and surface of maraging 13Ni15Co10Mo annealed in air at 900 °C for 1 h.

The OM, SEM, STEM, XRD, dilatometry and hardness analyses on the bulk region showed the presence of a single martensite phase. It is a lath martensite with all the solutes in solid solution and containing high density of dislocation tangles. The martensite was formed during cooling and the dilatometry curve indicated that the completed transformation occurred around 50 °C. It was measured a hardness of $401 \pm 6 \text{ HV1}$.

The SEM, EDS, XRD and GIXRD analyses were conducted in regions of different depth from the surface. The analyses showed the presence of different oxides (hematite, magnetite and kamiokite) and the austenite phase. The austenite is not a stable phase at room temperature in maraging 13Ni15Co10Mo. This occurs in this steel due the synergy between three factors:

- Increase in the austenite stabilization field, due to the cobalt content.
- Formation of kaminokite, hematite and magnetite oxides on the steel surface during exposure to high temperatures, due to the high Mo content.
- Migration of cobalt and nickel atoms towards the bulk during the formation of oxides.

Due to the low toughness of the maraging 13Ni15Co10Mo, the presence of a ductile austenite region on the surface, can open a window of scientific and technological opportunities for these steels.

Author Contributions: Conceptualization, N.B.d.L. and A.F.P.; methodology, D.P.M.d.F.; software, D.P.M.d.F.; validation, D.P.M.d.F., L.G.d.C., N.B.d.L. and A.F.P.; formal analysis, D.P.M.d.F.; investigation, D.P.M.d.F., N.B.d.L. and A.F.P.; resources, A.F.P.; data curation, D.P.M.d.F. and N.B.d.L.; writing—original draft preparation, D.P.M.d.F.; writing—review and editing, L.G.d.C., N.B.d.L. and A.F.P.; visualization, D.P.M.d.F.; supervision, A.F.P.; project administration, A.F.P.; funding acquisition, D.P.M.d.F. All authors have read and agreed to the published version of the manuscript.

Funding: This research was funded by National Council for Scientific and Technological Development (CNPq), grant number 168256/2018-5.

Data Availability Statement: Not applicable.

Acknowledgments: The authors would like to acknowledge the Molecular Foundry—Lawrence Berkeley National Laboratory (LBNL) and the National Institute of Metrology, Standardization and Industrial Quality (INMETRO).

Conflicts of Interest: The authors declare no conflict of interest.

References

1. Rao, M.N. Progress in Understanding the Metallurgy of 18% Nickel Maraging Steels. *Int. J. Mater. Res.* **2006**, *97*, 1594–1607. [[CrossRef](#)]
2. Floreen, S. Maraging Steels. In *Metals Handbook—VOLUME 1: Properties and Selection, Irons and Steels*; ASM International: Materials Park, OH, USA, 1978; pp. 445–452.
3. Hornbogen, E.; Rittner, K. Development of Thermo-Mechanical Treatments of a Maraging Steel for Yield Strengths above 3 GPa. *Steel Res.* **1987**, *58*, 172–177. [[CrossRef](#)]
4. Menzel, J.; Klar, H.-J. Systematische Gefügeuntersuchungen Am Martensitaushirtenden Stahl X 2 NiCoMo 13 15 10. *Steel Res.* **1990**, *61*, 30–38. [[CrossRef](#)]
5. da Fonseca, D.P.M.; Melo Feitosa, A.L.; de Carvalho, L.G.; Plaut, R.L.; Padilha, A.F. A Short Review on Ultra-High-Strength Maraging Steels and Future Perspectives. *Mater. Res.* **2021**, *24*, 20200470. [[CrossRef](#)]
6. Alves, T.J.B.; Nunes, G.C.S.; Tupan, L.F.S.; Sarvezuk, P.W.C.; Ivashita, F.F.; de Oliveira, C.A.S.; Paesano, A. Aging-Induced Transformations of Maraging-400 Alloys. *Metall. Mater. Trans. A Phys. Metall. Mater. Sci.* **2018**, *49*, 3441–3449. [[CrossRef](#)]
7. Viswanathan, U.K.; Dey, G.K.; Asundi, M.K. Precipitation Hardening in 350 Grade Maraging Steel. *Metall. Trans. A* **1993**, *24*, 2429–2442. [[CrossRef](#)]
8. He, Y.; Yang, K.; Qu, W.; Kong, F.; Su, G. Strengthening and Toughening of a 2800-MPa Grade Maraging Steel. *Mater. Lett.* **2002**, *56*, 763–769. [[CrossRef](#)]
9. Gawad, S.A.; Nasr, A.; Fekry, A.M.; Filippov, L.O. Electrochemical and Hydrogen Evolution Behaviour of a Novel Nano-Cobalt/Nano-Chitosan Composite Coating on a Surgical 316L Stainless Steel Alloy as an Implant. *Int. J. Hydrog. Energy* **2021**, *46*, 18233–18241. [[CrossRef](#)]
10. Baioumy, S.A.; Sanad, W.A.; El-Sherif, A.A.; Fekry, A.M.; Filippov, L.O. Electrochemical Behaviour and X-ray Fluorescence Study of AgNP-GO-CS Coated AISI 303 Austenitic Stainless Steel and Ceramic Commercial Products. *Int. J. Electrochem. Sci.* **2021**, *16*, 1–14. [[CrossRef](#)]
11. Bioumy, S.A.; Ahmed, R.A.; Fekry, A.M. Electrochemical Corrosion Behavior of Graphene Oxide/Chitosan/Silver Nanoparticle Composite Coating on Stainless Steel Utensils in Aqueous Media. *J. Bio-Tribo-Corrosion* **2020**, *6*, 78. [[CrossRef](#)]
12. Tammam, R.H.; Fekry, A.M. Corrosion Behavior of 316L Stainless Steel Coated by Chitosan/Gold/Nickel Nanoparticles in Mixed Acid Mixture Containing Inorganic Anions. *Int. J. Electrochem. Sci.* **2017**, *12*, 8991–9006. [[CrossRef](#)]
13. El-Salam, H.M.A.; El-Hafez, G.M.A.; Askalany, H.G.; Fekry, A.M. A Creation of Poly(N-2-Hydroxyethylaniline-Co-2-Chloroaniline) for Corrosion Control of Mild Steel in Acidic Medium. *J. Bio-Tribo-Corrosion* **2020**, *6*, 53. [[CrossRef](#)]
14. Klein, I.E.; Sharon, J.; Yaniv, A.E. A Mechanism of Oxidation of Ferrous Alloys by Super-Heated Steam. *Scr. Metall.* **1981**, *15*, 141–144. [[CrossRef](#)]
15. Klein, I.E.; Yaniv, A.E.; Sharon, J. The Oxidation Mechanism of Fe-Ni-Co Alloys. *Oxid. Met.* **1981**, *16*, 99–106. [[CrossRef](#)]
16. Greyling, C.J.; Kotzé, I.A.; Viljoen, P.E. The Kinetics of Oxide Film Growth on Maraging Steel as Described by Space-charge Effects. *Surf. Interface Anal.* **1990**, *16*, 293–298. [[CrossRef](#)]

17. de Souza Martins Cardoso, A.; da Igreja, H.R.; Garcia, P.S.P.; Chales, R.; Pardal, J.M.; Tavares, S.S.M.; da Silva, M.M.; Paesano, A.; Pichon, L. Structural Characterization of Iron Oxide Grown on 18% Ni-Co-Mo-Ti Ferrous Base Alloy Aged under Superheated Steam Atmosphere. *Int. J. Adv. Manuf. Technol.* **2022**, *119*, 1757–1768. [[CrossRef](#)]
18. Cerra Florez, M.A.; Ribas, G.F.; Cardoso, J.L.; Mateo García, A.M.; Roa Rovira, J.J.; Bastos-neto, M.; de Abreu, H.F.G.; da Silva, M.J.G. Oxidation Behavior of Maraging 300 Alloy Exposed to Nitrogen/Water Vapor Atmosphere at 500 °C. *Metals* **2021**, *11*, 1021. [[CrossRef](#)]
19. Klein, I.E.; Levitzky, M.; Sharon, J. Depth profile compositional analysis of thin oxide films on Fe-Ni-Co alloys by AES-ESCA techniques. *Corros. Rev.* **1984**, *6*, 97–117.
20. Rezek, J.; Klein, I.E.; Yahalom, J. Structure and corrosion resistance of oxides grown on maraging steel in steam at elevated temperatures. *Appl. Surf. Sci.* **1997**, *108*, 159–165.
21. Rezek, J.; Klein, I.E.; Yahalom, J. Electrochemical properties of protective coatings on maraging steels. *Corros. Sci.* **1997**, *39*, 385–397. [[CrossRef](#)]
22. Pfistermeister, M.; Krapf, H.; Coester, E. Process for the Formation of an Anticorrosive, Oxide Layer on Maraging Steel. U.S. Patent 4.141.759, 27 February 1979.
23. Vicente, A.d.A.; Brandi, S.D.; Padilha, A.F. Efeito Do Teor De Molibdênio Nas Curvas De Endurecimento Por Precipitação E Na Resistência À Oxidação a Altas Temperaturas De Aços Maraging De Ultra Alta Resistência Mecânica. *Tecnol. Metal. Mater. Mineração* **2015**, *12*, 179–187. [[CrossRef](#)]
24. Berns, H.; Theisen, W. *Ferrous Materials: Steel and Cast Iron*; Springer: Berlin, Germany, 2008; Volume 53, ISBN 9783540718475.
25. Carvalho, L.G.d.; Andrade, M.S.; Plaut, R.L.; Souza, F.M.; Padilha, A.F. A Dilatometric Study of the Phase Transformations in 300 and 350 Maraging Steels During Continuous Heating Rates. *Mater. Res.* **2013**, *16*, 740–744. [[CrossRef](#)]
26. Shashanka, R.; Chaira, D. Optimization of Milling Parameters for the Synthesis of Nano-Structured Duplex and Ferritic Stainless Steel Powders by High Energy Planetary Milling. *Powder Technol.* **2015**, *278*, 35–45. [[CrossRef](#)]
27. Nayak, A.K.; Shashanka, R.; Chaira, D. Effect of Nanosize Yittria and Tungsten Addition to Duplex Stainless Steel during High Energy Planetary Milling. *IOP Conf. Ser. Mater. Sci. Eng.* **2016**, *115*, 012008. [[CrossRef](#)]
28. Shashanka, R.; Chaira, D. Development of Nano-Structured Duplex and Ferritic Stainless Steels by Pulverisette Planetary Milling Followed by Pressureless Sintering. *Mater. Charact.* **2015**, *99*, 220–229. [[CrossRef](#)]
29. Khan, A.N.; Salam, I.; Tauqir, A. Formation of solid-state dendrites in an alloy steel. *Surf. Coat. Technol.* **2004**, *179*, 33–38. [[CrossRef](#)]
30. Bourgeot, J.; Maitrepierre, P.; Manenc, J.; Thomas, B. Hardening Fe-Ni-Mo and Fe-Ni-Co-Mo Martensitic Alloys by Tempering. IRSID Int. Rep. No 116. Part I: Electron Microscope Study of Coherent Precipitation in Fe-Ni-Co-Mo Maraging Alloys. In Proceedings of the 5th International Materials Symposium, Berkeley, CA, USA, 13–17 September 1971; University of California: Berkeley, CA, USA, 1971.
31. Florez, M.A.C.; Ribas, G.F.; Rovira, J.J.R.; García, A.M.M.; Lima, M.N.d.; Perdrix, G.R.; Cardoso, J.L.; da Silva, M.J.G. Production and Characterization of Oxides Formed on Grade 300 and 350 Maraging Steels Using two Oxygen / Steam Rich Atmospheres. *Mater. Res.* **2022**, *25*, 1–16. [[CrossRef](#)]